

# The Internal Kinematics of the Leo I Dwarf Spheroidal Galaxy: Dark Matter at the Fringe of the Milky Way \*

Mario Mateo<sup>1</sup>

e-mail: `mateo@astro.lsa.umich.edu`

Edward W. Olszewski<sup>2</sup>

e-mail: `edo@as.arizona.edu`

Steven S. Vogt<sup>3</sup>

e-mail: `vogt@ucolick.org`

Michael J. Keane<sup>4</sup>

e-mail: `mk@ctio.noao.edu`

Received \_\_\_\_\_; accepted \_\_\_\_\_

---

\*Based on observations obtained at the W.M. Keck Observatory, which is jointly operated by the California Institute of Technology and the University of California.

<sup>1</sup>Department of Astronomy, University of Michigan, 821 Dennison Bldg., Ann Arbor, MI 48109-1090

<sup>2</sup>Steward Observatory, University of Arizona, Tucson, AZ 85721

<sup>3</sup>Lick Observatory, University of California, Santa Cruz, CA 95064

<sup>4</sup>Cerro Tololo Interamerican Observatory, Casilla 603, La Serena, Chile

## ABSTRACT

We present radial velocities of 33 red giants in the Leo I dSph galaxy obtained from spectra taken with the HIRES echelle spectrograph on the Keck I telescope. These data have a mean precision of  $2.2 \text{ km s}^{-1}$  and lead to estimates of the central velocity dispersion and systemic velocity of Leo I of  $8.8 \pm 1.3 \text{ km s}^{-1}$ , and  $287.0 \pm 1.9 \text{ km s}^{-1}$ , respectively. The systemic velocity confirms past results that Leo I has an unusually large galactocentric velocity, implying the presence of a massive dark halo in the Milky Way or an extended dark component pervading the Local Group. The V-band ( $M/L$ ) ratio of Leo I is in the range 3.5-5.6. We have produced a set of models that account for the effects of stellar evolution on the global mass-to-light ratio of a composite population. Because Leo I contains a dominant intermediate-age population, we find that the V-band mass-to-light ratio of Leo I would be in the range 6-13 if it were composed exclusively of old stars such as found in globular clusters. This suggests that Leo I probably does contain a significant dark halo. The mass of this halo is approximately  $2 \times 10^7 M_{\odot}$ , similar to the dark halo masses inferred for all other Galactic dSph galaxies.

Because Leo I is isolated and has passed the Milky Way at most once in the past, external tides could not plausibly have inflated its central dispersion to the observed value. We also considered whether MODified Newtonian Dynamics (MOND) could account for the internal kinematics of Leo I and conclude that this alternative gravitational model can account for the Leo I kinematics adequately without requiring a dark halo. The agreement with MOND is particularly good if the velocity dispersion exhibits some anisotropy or the underlying stellar mass function is only slightly different than a classical Salpeter law.

## 1. Introduction

Over the past few years, there has been steady progress in obtaining reliable internal kinematic data for a number of the dwarf spheroidal (dSph) satellites of the Milky Way (see recent reviews by Olszewski 1998; Mateo 1997, 1998). One interesting result to emerge from these studies is that the minimum mass of a dSph system is about  $2.0 \pm 1.0 \times 10^7 M_\odot$ ; consequently, the lowest-luminosity dwarfs are also the ones with the largest ( $M/L$ ) ratios (Vogt et al 1995, Mateo 1997, 1998; Olszewski 1998). We have also learned that only one dSph, Ursa Minor, is convincingly rotating with  $v_{rot}/\sigma_0 \sim 0.5$  (Hargreaves et al. 1994; Armandroff et al. 1995). Binary stars have been detected among the red giants used for kinematic studies of dSph galaxies (Mateo et al. 1991; Olszewski et al. 1995; Queloz et al. 1995), but their effect on the derived masses of these galaxies has been shown to be negligible (Olszewski et al 1996; Hargreaves et al 1996). At present, reliable estimates of the central velocity dispersions have been obtained for all but one of the dSph satellites of the Milky Way (Mateo 1998). The lone exception – and the subject of this paper – is the outermost system, Leo I.

Because of its remote location in the outer halo of the Milky Way, Leo I is a particularly useful system to test whether tidal effects or dark matter can best explain the kinematics. Many models of the dynamical history of the Local Group reveal that the birthplace of Leo I was far from any large galaxies of the Local Group (Byrd et al 1994; Peebles 1989, 1995). It has also been suggested that Leo I, Leo II and some other Milky Way dwarfs constitute a single ‘stream’ of galaxies – mostly on the basis of their positions in the sky (Kunkel 1979; Lynden-Bell 1982; Majewski 1994). However, when the kinematics of the putative stream members are considered ( $v_{helio, Leo I} = 287 \text{ km s}^{-1}$ ;  $v_{helio, Leo II} = 76 \text{ km s}^{-1}$ ), the physical association is far less compelling (Lynden-Bell and Lynden-Bell 1995). Thus, Leo I appears to be a relatively isolated ‘test particle’, one whose internal kinematics are

unlikely to have been significantly affected by strong interactions with other systems.

Given our basic lack of understanding of the nature of the postulated dark matter in galaxies, and the interesting successes of MOdified Newtonian Dynamics (MOND) in explaining the properties of large galaxies (most recently by MacGaugh and de Blok 1998), it remains important to test this concept in dwarf systems. Although MOND’s scaling parameter (Milgrom 1983a,b) was set to match rotation curves of luminous galaxies, it has so far been consistent with the observations of dwarf spheroidal galaxies (Gerhard 1994; Milgrom 1995). Since MOND is falsifiable, one clearcut failure eliminates this model from further consideration (Kuijken and Gilmore 1989; Lake and Skillman 1989; Milgrom 1990). Because the internal gravitational accelerations within Leo I are comparable to the limit where MOND is postulated to be applicable, we can investigate here how well MOND accounts for the internal kinematics of yet another low-mass dwarf system.

This study represents the final chapter in the reconnaissance of the kinematics of the known dwarf spheroidal companions of the Milky Way (see Mateo 1998 for a review). However, we are on the threshold of an era of similar kinematic studies of more distant galaxies throughout the Local Group and of far more extensive kinematic studies of our closest neighbors. In two subsequent papers, we shall explore the kinematics of LGS 3 – a companion of M 31 – and carry out an extensive study of the kinematics of Leo I using fiber spectroscopy of over 100 red giants in the galaxy (Cook et al 1998; Mateo et al. 1998, hereafter Paper III).

Throughout this paper we report all mass-to-light ratios in solar units.

## 2. Observations and Reductions

The data used in this study were obtained with the HIRES spectrograph (Vogt et al. 1994) on the Keck I 10m telescope during the nights of March 13-14 (UT), 1996. The observing and reduction procedures we used are identical to those described in detail by Vogt et al (1995, hereafter Paper I).

Table 1 provides a log of our observations; a total of 40 spectra of 33 different Leo I candidate red giants were obtained. These candidates were selected from a color-magnitude diagram of the central regions of Leo I obtained with the Michigan-Dartmouth-MIT Hiltner 2.4m telescope in December 1992. This diagram is reproduced in Figure 1 which also shows the selection criteria used to isolate candidate Leo I members. Since Leo I has a systemic velocity of about  $286 \text{ km s}^{-1}$  (Zaritsky et al 1989; Kulessa and Lynden-Bell 1992; Section 3.1) in a direction where the Sun’s reflex velocity due to Galactic rotation is about  $100 \text{ km s}^{-1}$ , it is evident from Table 1 that every star we observed is in fact a near-certain member of the galaxy. Unlike the situation for Fornax (Mateo et al. 1991), there is no kinematic ambiguity about membership. Nor are there any foreground red-dwarf contaminants as in the case of Carina (Mateo et al 1993). Leo I is located at a relatively high Galactic latitude ( $b = 49.1$ ) and its compact angular size improves the contrast of members with respect to field stars. The locations of the stars we observed are shown in Figure 2. Figure 3 illustrates the velocity distribution of all stars in our radial velocity sample for Leo I.

We used the MDM photometric observations to obtain calibrated Johnson V-band and Kron-Cousins I-band photometry of all of the spectroscopically observed stars. These frames along with data obtained with the Palomar 1.5m telescope in 1991 were used to determine precise coordinates for each star (details of this process will be described in Paper III where we present fiber spectroscopy of nearly 100 Leo I members). We then

calculated the position angle and angular distance of each star from the center of the galaxy (taken to be  $\alpha_{2000} = 10^h08^m27.93^s$ ,  $\delta_{2000} = 12^\circ18'18.4''$ ). These photometric and astrometric results are provided in Table 2 for each star that we observed.

The velocities and  $R$  values (as defined by Tonry and Davis 1979) listed in Table 1 for each spectrum were obtained using the `fxcor` package in version 2.10 of IRAF. This routine uses a Fourier cross-correlation algorithm to estimate velocities relative to a high-S/N template spectrum. Our template was composed of high-quality spectra of numerous bright radial-velocity standards shifted to a common velocity system. We have found in many past studies that the formal errors returned by `fxcor` are overly optimistic by factors of 2-5. To better estimate the errors, we used our repeat observations of six of the Leo I stars, three stars in LGS 3 (Cook et al. 1998), and multiple observations of standard radial velocity stars to calculate the proportionality constant,  $A$ , for the relation

$$\delta_i = A/(1 + R_i) \quad (1)$$

via a least-squares minimization technique (see Paper I for details). In equation 1,  $\delta_i$  and  $R_i$  are the formal error from `fxcor` and the Tonry-Davis  $R$  statistic for star  $i$ , respectively. This process gave  $A = 14.9 \text{ km s}^{-1}$ . Our estimates for the mean velocities and velocity errors for the 33 stars we observed in Leo I are listed in Table 2. The final mean velocities were determined by weighting the individual measurements by  $\delta_i^{-2}$  for stars with multiple observations.

### 3. Results

#### 3.1. The central velocity dispersion of Leo I

The kinematic data listed in Table 2 can be used to calculate the velocity dispersion,  $\sigma_v$ , of Leo I. The basic procedure has been described in Paper I and in reviews by Pryor

(1992) and Mateo (1997).

The core radius of Leo I is 3.3 arcmin (see Table 4). Only one star in our sample is located further from the center of Leo I (star 1,  $r = 3.5$  arcmin) and the average angular separation of the stars we observed from the center of the galaxy is 1.9 arcmin. Therefore, we shall consider the velocity dispersion of our sample to be equivalent to the central velocity dispersion of Leo I; any corrections are model-dependent and will be explored in detail in more comprehensive models in Paper III.

We have used here three model-independent estimators to calculate  $\sigma_v$ . The first is the weighted standard deviation as defined by Mateo et al (1991, 1993) and in Paper I:  $\sigma_{v,wm} = 8.6 \pm 1.2 \text{ km s}^{-1}$ . This value explicitly accounts for the different velocity errors for each star. The second estimator is known as the bi-weight and is designed to be more robust than a weighted standard deviation by minimizing the contribution of outliers (Beers et al 1990). For our observations,  $\sigma_{v,bi} = 9.2 \pm 1.6$ , where the error represents a 90% confidence limit. For this estimator, we gave each star equal weight. Finally, a maximum likelihood estimator was used to calculate the central dispersion as described by Olszewski et al. (1996) and Armandroff et al. (1995). For this case, we derived  $\sigma_{v,ml} = 8.8 \pm 1.3$ . It is clear that all three techniques provide essentially identical estimates of  $\sigma_v$  for our full sample.

We have searched for dependencies of the velocity dispersion for different subsamples of stars. Table 3 lists  $\sigma_v$  and systemic velocities ( $\langle v \rangle$ ) for (a) AGB stars: the 18 stars brighter than  $I = 18.1$ , (b) RGB stars: 15 stars fainter than  $I = 18.1$ , (c) the innermost third of the sample: the 11 stars closest to the center of Leo I, (d) the middle third of the sample: 11 stars, (e) the outermost third of the sample: 11 stars, (f) the innermost half of the sample: 16 stars, (g) the outermost half of the sample: 17 stars, (h) the ‘eastern’ sample: 16 stars, and (i) the ‘western’ sample: 17 stars. These eastern and western sample are defined with respect to the least-squares rotation solution based on equation 2 and described below in

section 3.2.

To determine whether any of the differences in the velocity dispersions of the various samples are statistically significant, we also determined  $\sigma_v$  and  $\langle v \rangle$  for randomly-selected samples of 11 and 16 stars drawn from the full dataset. In each case, we list the 5% and 95% values in these distributions; for a normal distribution these percentile limits approximately correspond to 2-sigma deviations from the mean. These random samples suggest that virtually none of the differences seen in the dispersions for the subsamples listed in Table 3 are statistically significant at greater than a 2-sigma level. For example, the rather large velocity dispersion of the outer-half sample is exceeded about 6% of the time by a random sample of 16 stars. Of course, the outer and inner samples are strongly anti-correlated: If one subsample exhibits a relatively large dispersion relative to the mean dispersion for all stars, the other subsample must exhibit a small value. We conclude from Table 3 that there are no obvious variations in the kinematic properties of Leo I as a function of stellar type or location. The only possible exception is the bi-weight estimate of the dispersion from the outer-third sample:  $\sigma_v = 4.7 \pm 1.4 \text{ km s}^{-1}$ . In this case, the bi-weight ignored (by design) two of the stars with velocities furthest from the mean. Since the other two dispersion estimators obtained significantly larger values for  $\sigma_v$ , we attach little significance to this one case.

Figure 4 is a plot of the observed radial velocities as a function of stellar magnitude, color, radial distance, and position angle. There is no apparent trend visible in any of these plots, a conclusion that is confirmed from least-squares fits of straight lines to these data. In each case, the 2-sigma formal error of the best-fit slope is larger than the slope itself.

Our adopted value for the mean central velocity dispersion of Leo I is based on the full sample of stars for which we derive  $\sigma_{v,0} = 8.8 \pm 1.3 \text{ km s}^{-1}$ . This value is the average of the three estimates listed on the first line of Table 3, weighted by  $\delta^{-2}$ . We shall use this value



in our subsequent discussion where we estimate the central mass density and total mass of Leo I.

### 3.2. Rotation of Leo I

Paltoglou and Freeman (1987) suggested that the presence of significant rotation in dSph galaxies could be used as a means of testing whether these systems evolved from dIrr galaxies via ram-pressure stripping, or perhaps by blow-out during energetic star-formation episodes. To date, the only dSph galaxy that exhibits evidence of significant rotation is Ursa Minor (Hargreaves et al. 1994; Armandroff et al. 1995; Mateo 1998). Since UMi is the closest dSph, it is possible that tidal effects could cause streaming motions that can mimic rotation (Piatek and Pryor 1995; Oh et al. 1995; Johnston et al. 1995), although the apparent rotation axis is not consistent with this explanation (Armandroff et al. 1995). Tidal effects are negligible for Leo I (see section 5.2) since it is located far from the Milky Way.

We used two algorithms to try to detect bulk rotation in Leo I. First, we sorted the stars by position angle, then used each star to define an axis passing through its position and the galaxy center. We then calculated the mean velocity and dispersion on either side of this axis and calculated the mean velocity difference (and formal error of the difference) of the two sides. In no case did the velocity difference exceed 0.7-sigma from which we conclude there is no detectable rotation.

The second approach was to perform a least-squares fit to a cylindrical solid-body rotation curve:

$$v_i = v_0 + S_v R_i \cos \theta_i, \quad (2)$$

where  $v_0$  is the systemic velocity,  $S_v$  is the rotational velocity gradient,  $R_i$  is the radial

distance of star  $i$  from the galaxy center, and  $\theta$  is the angle between the position angle of a star  $i$  and the line that is normal to the rotation axis and passes through the galaxy center. In order to transform this into a linear least-squares problem, we determined  $S_v$  for different assumed rotation axes in increments of 0.1 deg. The best fit gave an inferred rotation axis 144.1 deg (measured from north through east) and a systemic velocity of 287.4 km s<sup>-1</sup>. However, for this fit  $\chi^2_{min} = 18.3$  (per degree of freedom), and the formal error of the rotation gradient was  $0.017 \pm 0.0096$  km s<sup>-1</sup> arcmin<sup>-1</sup>. The mean velocity difference of stars on both sides of the best-fit rotation axis is listed in Table 3 for the three velocity estimators; in no case is the difference larger than 1.1-sigma. These results suggest that the detected ‘rotation’ is statistically insignificant. This is visually confirmed in Figure 5 which shows the Leo I radial velocities versus the radial separation projected onto the axis of maximum gradient for the best-fit rotation solution (which is also shown with its formal error). Also plotted in Figure 5 is the reduced  $\chi^2$  as a function of rotation position angle showing the small variation and large mean value of this statistic.

These negative results do *not* rule out global rotation in Leo I. Since the galaxy exhibits a relatively large central velocity dispersion and because our sample subtends a limited radial distribution, mostly within one core radius of Leo I, we would have only been able to detect rotation in the presence of a rapidly rising rotation curve of moderate amplitude. A more definitive discussion of the rotation of Leo I requires a larger, more extended sample of giants (Paper III).

### 3.3. The systemic velocity of Leo I

As with the velocity dispersion, we have used a weighted mean, the biweight, and the maximum likelihood technique to estimate the systemic velocity of Leo I. The results for the full sample are:  $\langle v \rangle_{wm} = 287.3 \pm 1.6$  km s<sup>-1</sup>,  $\langle v \rangle_{bi} = 286.7 \pm 2.0$  km s<sup>-1</sup>,  $\langle v \rangle_{ml} = 287.0 \pm 1.6$

km s<sup>-1</sup>. The systemic velocity of Leo I is listed for various other subsamples in Table 3. The rotation analysis in the previous section also provides an estimate of the systemic velocity:  $v_{sys,rot} = 287.4$  km s<sup>-1</sup>. We also explored the possibility that the systemic velocity might prove to be a function of stellar subsample in our dataset; Table 3 and Figure 3 illustrate that the systemic velocity of Leo I does not significantly depend on subsample. In particular, no subsample exhibits a systemic velocity outside the 90% confidence limits determined from our Monte-Carlo simulations. For comparison, Zaritsky et al. (1989) obtained a mean velocity of  $285 \pm 2$  km s<sup>-1</sup> from 10 observations of six stars, while Kulessa and Lynden-Bell (1992) report a mean heliocentric velocity of 290 km s<sup>-1</sup> but with no details or error estimate. We confirm these earlier estimates of the systemic velocity of Leo I.

Zaritsky et al. (1989) showed that a modified timing argument including the Milky Way, M 31 and Leo I gave a result consistent with the classical timing argument, namely, that the Milky Way mass must be large. This model assumes that Leo I receded from its original galactocentric distance from universal expansion, approached the Milky Way because of the overdensity of the Local Group, and is now receding on a bound orbit. Models in which Leo I is unbound to the Milky Way but remains bound to the Local Group (Byrd et al. 1994) also require a considerable dark matter component spread throughout the volume of the group. It seems clear that a satisfactory understanding of the large systemic velocity of Leo I requires a comprehensive model of the entire Local Group, perhaps also including the past effects of galaxies now located in external, nearby groups (e.g. Peebles 1989, 1995).

#### 4. The Mass and Mass-to-Light Ratio of Leo I

Because our new observational data consist exclusively of velocities of stars located close to the center of Leo I, we shall only consider single-component dynamical models in this paper. We will consider single- and two-component models in Paper III where we analyze less precise velocity measurements of a larger sample of stars located well beyond the core radius of the galaxy.

By ‘single-component’ we mean that the mass distribution is assumed to follow that of the visible component. The latter is determined from star counts or surface brightness measurements. A unique complication in determining the structure of Leo I is its proximity in the sky to the bright star Regulus (Hodge 1971). The most recent study (Irwin and Hatzidimitriou 1995; hereafter IH95) used deep star counts on Palomar Schmidt plates; the structural parameters they derived are listed in Table 4 along with additional parameters from other sources.

The standard analysis for a single-component model – often referred to as the ‘core-fitting’ or King’s method (King 1966) – is described by Richstone and Tremaine (1986) who further adopt an assumption of isotropy in the velocity distribution. Pryor and Kormendy (1990; hereafter PK90) explore the effects of an anisotropic velocity distribution on the final mass and ( $M/L$ ) ratio for single- and two-component models where the visible and dark component, if any, can have distinct spatial extents. Though we shall deal with single-component models here, we use the results from PK90 below to set a lower limit on the central mass density of Leo I in extreme two-component models.

The basic analysis in this paper follows that of Paper I where we used the following relations:

$$\rho_0 = 166\sigma_0^2\eta/R_{1/2}^2, \quad (3)$$

$$M_{tot} = 167 R_c \beta v_s^2, \quad (4)$$

$$I_0 = S_0 / 2.1 R_{1/2}, \quad (5)$$

which explicitly assume that mass follows light and that the velocity distribution is isotropic (see King 1966; Richstone and Tremaine 1986; Kormendy 1987; PK90 for details on the basis of these relations). The quantities  $\rho_0$ ,  $M_{tot}$ , and  $I_0$  are the central mass, total mass, and luminosity density for the model, respectively.  $\sigma_0$  is the central velocity dispersion as defined in Table 3, while  $v_s$  is the so-called ‘scale velocity’ defined by PK90.  $S_0$  is the central surface brightness, expressed in units of  $L_\odot \text{pc}^{-2}$ , while  $R_c$  and  $R_{1/2}$  are the King core radius and half-surface brightness radius, respectively. The other factors and parameters ( $\eta$ ,  $\beta$ , and the scaling factor relating  $v_s$  and  $\sigma_0$ ) are taken from the appropriate King models that best fit the star-count profile of Leo I. In all cases, the radii are geometric means, defined as  $R_{geom} = R_{maj}(1 - e)^{1/2}$ , where  $e$  is the ellipticity of the galaxy,  $e = 1 - R_{min}/R_{maj}$ . The concentration of Leo I is defined as  $\log R_t/R_c = 0.58$ , where  $R_t$  is the tidal radius; the appropriate values of the various parameters for this model are also listed in Table 4 for the isotropic case. Note that if we retain the assumption that mass follows light but drop the assumption of isotropy, the final effect on the inferred mass and central density is relatively slight ( $\sim 50\%$  lower values of  $\rho_0$  and  $M_{tot}$ ; Merritt 1988; PK90); however, in this case there is no guarantee that the resulting models will be dynamically stable (Binney and Mamon 1982; Merritt 1988).

Table 5 lists the masses and  $(M/L)$  ratios we derive for Leo I using King’s method and our new estimate of the central velocity dispersion.

## 5. Discussion

### 5.1. The Case for Dark Matter in Leo I

The results in Table 5 do not strongly support the notion that Leo I contains a dominant DM component. A mass-to-light ratio of 4-8 is smaller than values observed in more extreme cases of DM in dSph systems such as Draco, Ursa Minor, Carina, or Sextans where  $(M/L)$  ratios ranging from 50-100 are seen (see Mateo 1998 for a review). And although the  $(M/L)$  ratio we find for Leo I is larger than the mean value observed in low-concentration globular clusters –  $\langle(M/L)_{0,V} = 1.51 \pm 0.10$  – the difference is only barely significant at the 2-sigma level<sup>6</sup>. Armandroff and Da Costa (1986) explored the range of  $(M/L)$  ratios for pure stellar populations comprised only of stars, their remnants, for a range of power-law initial mass functions. They concluded that such populations can produce V-band  $(M/L)$  values as high as 5-6, though such extreme values for  $(ML)$  required steep mass functions dominated by low-mass stars, or shallow mass functions that produce many massive, but dark remnants from high-mass stars. For a Salpeter mass function, the upper limit on  $(M/L)_V$  is about 2.5, just consistent with the lowest value derived here for Leo I (Table 5).

---

<sup>6</sup>The results for the globular clusters are taken from the 36 clusters with concentration parameters  $\leq 2.0$  compiled by Pryor and Meylan (1993). Internal dynamical effects may significantly alter the core stellar populations, and hence the  $(M/L)$  ratios, in more concentrated clusters (Djorgovski et al. 1991; Shara et al. 1998). The mass-to-light ratios we have adopted from the compilation by Pryor and Meylan (1993) were determined for the globular clusters in their sample techniques similar to the core-fitting method we have adopted for for Leo I in this study. These authors also list ‘total’  $(M/L)$  ratios for the clusters in their sample but these were determined using a considerably more elaborate model than the simple King method we use in section 4. Thus, we shall exclusively compare the former globular-cluster  $(M/L)$  ratios with our results for Leo I and the other nearby dSph galaxies.

There is an important complication in this discussion in the case of Leo I. Lee et al. (1993) and Gallart et al. (1998) have determined that Leo I contains a significant young population. Because main sequence stars obey a steep mass-luminosity relation ( $L \propto m^3$ ) and because stellar remnants have extremely high ( $M/L$ ) ratios, the global ( $M/L$ ) ratio of a composite population increases with time (e.g., Elson et al. 1989).

How does the aging of a stellar population alter the global ( $M/L$ ) ratio of a galaxy with a complex star-formation history (SFH) such as Leo I? To answer this, we have estimated mass-to-light ratios for a composite stellar population formed from a reasonable stellar mass function and for a SFH consistent with that observed for Leo I (Gallart et al. 1998). The adopted SFH is shown schematically in the first panel of Figure 6 (taken from Mateo 1998). Our models involve timesteps of 10 million years during which a sub-population of stars is born with a mass spectrum of the form  $dN(m) \propto m^{-x} dm$  and upper and lower stellar mass limits,  $m_u$  and  $m_l$ , respectively. One set of models uses a single power-law mass function corresponding to the Salpeter slope,  $x = 2.35$ , from  $0.07 M_\odot$  to  $30 M_\odot$ . A second, ‘composite’ mass function takes the Salpeter slope for  $m \geq 0.3 M_\odot$  but then switches to  $x = 0.0$  for  $0.07 M_\odot \leq m \leq 0.30 M_\odot$ . Stars more massive than  $8 M_\odot$  are assumed to evolve into  $1.4 M_\odot$  neutron stars, while stars less massive than  $8 M_\odot$  become  $0.6 M_\odot$  white dwarfs at the end of their lifetimes. Both sorts of remnants are assumed to have negligible luminosity. The main-sequence lifetimes of the stars are taken to be proportional to  $M^{-2.5}$  – consistent with the mass-luminosity relation above – and we assume the solar lifetime to be 10 Gyr.

We have tried to account for the contribution of red giants (which have low ( $M/L$ ) ratios) using two parameters. First, to constrain the total number of giants we simply assumed that 0.5% of the total number of the most massive stars that have not yet turned into remnants in a single star-formation episode will be seen as giants today. This procedure

fails for very young populations (age  $\lesssim 1$  Gyr) since the form and mean luminosity of the giant and red supergiant branches evolve rapidly for smaller ages (Mermilliod 1981; Ferraro et al. 1995). In addition, the red giant luminosities are constrained to be a factor,  $\gamma_L$ , times the luminosity of stars at the main-sequence turnoff (MSTO) point.

Because the red giant region in the CMD does not evolve rapidly with age for populations older than about 1 Gyr,  $\gamma_L$  is likely to vary with time as the MSTO luminosity steadily drops with increasing age. To calibrate this behavior, we have used the models of Elson et al. (1989) who studied the evolution of the mass-to-light ratio of single-aged populations. For their oldest models (12-14 Gyr), Elson et al. (1989) predicted V-band mass-to-light ratios ranging from 4-20 instead of 1-2 as observed in globular clusters. In practice, we found that if we let  $\gamma_L$  vary linearly between 25 at 1 Gyr, and 75 for ages  $\geq 10$  Gyr, our models produce a  $(M/L)$ -age relation for single-age populations that closely matches the slope of the same relation calculated by Elson et al. (1989) *and* achieve  $(M/L) \sim 1.5$  for old (14 Gyr) stars. It would clearly be useful to repeat this calculation with a complete set of modern evolutionary models to self-consistently account for the role of giants in the evolution of the  $(M/L)$  ratio. However, our approach allows us to rapidly explore how a complex star-formation history affects the evolution of a system’s mass-to-light ratio.

Table 6 summarizes the results of our models where we have explored the role of the mass function and star-formation history on the  $(M/L)$  ratio of three sample populations. The first, labeled ‘globular’, is a system in which constant star formation occurred only from 12-14 Gyr ago. The second, labeled ‘young’, is a population where the stars formed at a constant rate from 1-2 Gyr ago. Finally, we include results for a SFH appropriate to Leo I. These three SFHs are shown in the top row of Figure 6. We also list in the final column of Table 6 a parameter denoted as  $\lambda$ ; this is the ratio of the  $(M/L)$  ratio for the



globular cluster population divided by the  $M/L$  ratio of the other populations for the same mass function.

We can see in Table 6 that  $\lambda$  varies from about 1.75-2.31 for Leo I, depending on the form of the IMF. This is the factor by which the observed  $(M/L)$  ratio for Leo I must be multiplied to compare the results for this galaxy with the  $(M/L)$  ratio of a typical globular cluster. For the present discussion, we adopt the average of the results in Table 6,  $\lambda_{LeoI} = 2.03 \pm 0.3$ . This implies that the V-band  $(M/L)$  ratio of Leo I would range from about 6-13 if it were composed only of stars similar to those found in globular clusters (see Table 5). We conclude that Leo I does in fact contain a significant dark component.

We have calculated correction factors for the other dSph systems with core kinematic measurements using the schematic star-formation histories compiled by Mateo (1998); the adopted SFHs are plotted in Figure 6. These results are also listed in Table 6 for both the Salpeter and composite mass functions. Also listed in the table are the approximate values of the central  $M/L$  ratios for these galaxies corrected for population effects and converted to a scale on which the  $(M/L)_V$  ratio of the globular cluster population (as defined above) is  $\sim 1.5$ .

In Figure 7a we show the V-band  $(M/L)$  ratios vs the V-band luminosities of the nine Galactic dSph galaxies and the three luminous M 31 dSph systems with kinematic data (NGC 147, NGC 185, and NGC 205). These results have not been corrected for evolutionary effects. In Figure 7b we plot the corrected  $(M/L)$  ratios and corrected luminosities for the Galactic dSph systems using the mean  $\lambda$  values determined from Table 6; we applied no corrections to the M 31 satellites. The galaxy luminosities have also been corrected by the appropriate factor ( $\lambda^{-1}$ ) prior to plotting them in Figure 7b. These corrected  $(M/L)$  ratios correspond to the values these galaxies would have if their entire stellar mass could be converted to a population appropriate for a globular cluster and with the same stellar

mass function.

Apart from Sgr (see Section 5.2), the data plotted in both panels of Figure 7 are consistent with a simple model in which the galaxy  $(M/L)$  ratios can be fit to a relation of the form

$$(M/L) = (M/L)_s + M_{DM}/L, \quad (6)$$

where  $(M/L)_s$  is the intrinsic  $(M/L)$  ratio of the stellar population in the galaxy,  $M_{DM}$  is the mass of the underlying dark halo, and  $L$  is the total V-band luminosity in solar units. The best-fitting relations are shown in Figure 7. For both panels, we find  $M_{DM} \sim 2.0 \times 10^7 M_\odot$  for  $(M/L)_s = 1.5$ . The function described in equation 7 is plotted in Figure 7 for these values. Leo I fits this relation well in both plots. Whatever mechanism controls the location of a galaxy in the  $(M/L)$ - $M_V$  plane seems to also be at work in Leo I. It appears that all dSph systems contain dark matter, and that these dark halos are remarkably uniform. We take this as further evidence that Leo I has a dark component of similar basic properties as those found in other dSph systems.

## 5.2. The Case for Tidal Heating in Leo I

Kuhn and Miller (1989), Kuhn (1993), Kroupa (1997), and Klessen and Kroupa (1998) have argued that tidal effects can induce resonances in dSph systems that can artificially inflate their central velocity dispersions, hence mimicking dark matter. Pryor (1996) has argued from a theoretical standpoint that such heating is difficult to understand as an explanation for the large central velocity dispersions observed in dSph galaxies. Detailed  $n$ -body simulations of encounters of dSph galaxies and the Milky Way at impact parameters ranging from 10-50 kpc (Piatek and Pryor 1995; Oh et al. 1995; Johnston et al. 1995) suggest that close encounters can produce streaming motions in outer parts of the dwarfs. These motions will be seen as a systematic change of the mean velocity along the major

axis and can be incorrectly interpreted as rotation. Despite this streaming in the outer regions of the dwarfs, such close encounters negligibly alter the central velocity dispersion. Although strong evidence for tidal extensions and perturbations in some of the nearby dSph systems is accumulating rapidly (Mateo et al. 1996; Alard 1996; Fahlman et al. 1996; Kuhn et al. 1996; Kleyna et al. 1998), there are no convincing demonstrations yet of strong tidal heating of the core of a dSph galaxy, apart from the Sgr system which appears to be in the process of tidal disruption as it passes extremely close to the Milky Way (Bellazzini et al. 1996; Mateo 1998; Mateo et al. 1998; though see Ibata et al. 1997).

The central dispersion and inferred central ( $M/L$ ) ratio of Leo I is considerably higher than we would have expected in the absence of dark matter or tidal heating. However, the remote location and large systemic velocity of Leo I makes it difficult to understand how tides could have had a role in this result. Byrd et al. (1994) have specifically modeled the orbit of Leo I within the Local Group over a Hubble time. They argue that the galaxy has passed only one large system – the Milky Way – in its entire lifetime, about 2-4 Gyr ago. This is consistent with the rather small tidal radius of Leo I ( $\sim 1$  kpc; see Table 4) which was presumably established at the galaxy’s closest approach to the Milky Way ( $\sim 70$  kpc according to Byrd et al. 1994, though IH95 suggest that perigalacticon for Leo I was about 20-30 kpc). Models by Peebles (1989, 1995), though different in detail, likewise suggest that Leo I has had at most one past encounter with a large galaxy of the Local Group. These results are completely at odds with any resonance heating mechanism: In models by Kuhn and Miller (1989) and Klessen and Kroupa (1998), significant core heating does not occur until a galaxy has experienced several orbits around the Galaxy on timescales  $\lesssim 1$  Gyr.

We conclude that tides have not had a significant role in heating the core of Leo I. Their effect can be ruled out as the source of the large inferred ( $M/L$ ) ratio of that galaxy.

### 5.3. The Case for MOND in Leo I

The persistent lack of hard evidence regarding the true nature of dark matter has become sufficiently irksome that astrophysicists have begun to question even the most basic assumptions of our analysis in Section 5.1. One example is known as MODified Newtonian Dynamics (MOND) in which Newton’s law of gravity is modified to include a repulsive term at low accelerations. The reader interested in the surprising success of this model to explain galaxy kinematics and some discussions on the rather far-reaching implications of this idea is referred to Bekenstein and Milgrom (1994), Felton (1984), Sanders (1997), and McGaugh and de Blok (1998); though see Lake and Skillman (1989) and Kuijken and Gilmore (1989). In this section, we simply consider if MOND can account for the kinematics of Leo I without resorting to DM.

Milgrom (1995) defined a parameter  $\eta = (3\sigma_0^2/2R_c)/(V_\infty^2/R)$ , where  $\sigma_0^2$  is the central velocity dispersion of a dwarf galaxy,  $R_c$  is its core radius, and  $R$  is its distance from the center of the Galaxy.  $V_\infty$  is the asymptotic circular rotation speed at a distance  $R$ , taken here to be  $220 \text{ km s}^{-1}$ . The parameter  $\eta$  is thus a measure of the ratio of the internal and external gravitational accelerations; in the case of Leo I we obtain  $\eta = 2.5$  implying that this galaxy can be treated as an isolated system. The appropriate MOND relation to apply in this case is

$$M_{tot,MOND} = 81\sigma_0^4/4a_0G, \quad (7)$$

where  $a_0 = 1.2 \times 10^{-8} \text{ cm s}^{-2}$  is the MOND acceleration parameter derived from observations of rotation curves of giant disk galaxies (Milgrom 1983a,b; Milgrom 1998), and  $G$  is the gravitational constant. All terms in Equation 7 are in cgs units for the value of  $a_0$  noted above. If we adopt  $\sigma_0 = 8.8 \pm 1.3 \text{ km s}^{-1}$  (Table 4), then  $M_{tot,MOND} = 7.6 \pm 4.5 \times 10^6 \text{ M}_\odot$ . For the ‘total’ V-band luminosity listed in Table 5, this corresponds to  $(M/L)_V = 1.6 \pm 1.1$  where the error reflects the uncertainty in  $\sigma_0$  and  $L_V$ .

In Section 5.1 we argued that the present-day V-band  $(M/L)$  ratio of Leo I should be in the range 0.4-0.8 on a scale where a globular-cluster population has  $(M/L)_V \sim 1$ -2. The MOND  $M/L$  ratio is very slightly higher than this. One could interpret this to mean that Leo I requires a dark component even with MOND. Like the relations we used in Section 4 to apply King’s method to Leo I, Equation 7 assumes an isotropic velocity distribution and that mass follows light. The second assumption follows immediately in MOND since there is no dark component that might be distributed differently from the luminous material. However, an anisotropic velocity field may modify the inferred MOND mass estimate. If the arguments of PK90 for models where mass follows light and strictly Newtonian gravity are valid for MOND, then the total mass and central mass densities of an anisotropic MOND model may be about 2 times smaller than for the isotropic case (see section 6). This implies  $(M/L)_V \gtrsim 0.8 \pm 0.3$ , consistent with the expected value of 0.5-0.8, and certainly so if the underlying mass function is only slightly steeper or shallower than the Salpeter law (see section 5.1).

We conclude that MOND plausibly accounts for the internal kinematics of Leo I without the need for any DM. Lake & Skillman (1989) argued that MOND does not alleviate the need for DM in the rotating Local Group dwarf irregular galaxy IC 1613 and Kuijken and Gilmore (1989) suggest that the motions of stars perpendicular to the Galactic disk are also at odds with MOND and direct observations of the minimum disk surface mass density in the solar neighborhood. However, we stress that none of these cases represent fatal deviations from MOND predictions. Milgrom (1990) argued that inclination and distance uncertainties for IC 1613 are sufficiently large to remove the discrepancy with MOND. In Leo I the agreement with the MOND prediction is sufficiently good that only a small degree of anisotropy or a slightly modified mass function brings our observations and the MOND prediction into remarkably good agreement.

## 6. Summary and Conclusions

We have obtained precise radial velocities of 33 giants in the remote dSph galaxy Leo I using the HIRES echelle spectrograph on the Keck I telescope. These observations represent the final chapter of the reconnaissance of the central kinematic properties of the Galaxy’s satellite dSph systems (Mateo 1998).

Using King’s method, we derive a central V-band mass-to-light ratio of  $3.5 \pm 1.4$ , or a ‘total’  $(M/L)_V$  of  $5.6 \pm 2.1$  (see Table 5). These values are only slightly higher than the mean mass-to-light ratio observed in Galactic globular clusters ( $1.51 \pm 0.10$ ; Pryor and Meylan 1993). However, this simple comparison is not entirely valid because Leo I is dominated by a relatively young stellar population. To determine the magnitude of this effect, we generated a set of simple models to account for stellar evolution on the  $(M/L)$  ratio of a composite system. On a scale where the globular-cluster mass-to-light ratios are in the range 1-2, we find that the V-band  $(M/L)$  ratio of Leo I is in the range 6-13. Thus, we conclude that Leo I does appear to contain a significant dark component.

The properties of the dark halo inferred for Leo I closely match those found in other Galactic dSph systems (see Figure 7). We find no evidence for rotation in Leo I, nor any significant dependence of the kinematics on stellar type or location in the galaxy. However, we have relatively little leverage on rotation or spatial variations of the kinematics of Leo I because our rather small sample of 33 stars is almost entirely located within one core radius of the center of Leo I. Our results confirm earlier findings that the minimum mass of dSph systems appears to be about  $2.0 \times 10^7 M_\odot$ . Astronomers have yet to discover any galaxy, anywhere in the local Universe with a kinematically determined mass smaller than this (Lo et al. 1993 Young and Lo 1996, 1997a,b; Mateo 1998).

We have considered whether tides or MOdified Newtonian Dynamics (MOND) might account for the internal kinematics of Leo I. This galaxy is a good test case for tides and

MOND because it is well isolated from any external gravitational effects from the Milky Way. Because Leo I has had only one moderately close passage to any large galaxy (Byrd et al. 1994), we conclude that tides or tidal resonances are unlikely to have produced the kinematics we see in the galaxy. We also find that MOND can plausibly account for the internal kinematics of Leo I without the need for DM. This is especially true if there is a small degree of velocity anisotropy in the galaxy, or if its underlying stellar mass function is only slightly steeper or shallower than a classical Salpeter law.

Much of our analysis implicitly assumes that the stellar velocities are isotropically distributed in Leo I and, in the dark-matter models, that mass follows light. PK90 explored the effects of relaxing these assumptions for Ursa Minor and Draco. In particular, the lowest possible central mass density in a system such as Leo I corresponds to a highly anisotropic case where the dark matter is much more extended than the visible material (Merritt 1988). Using the same assumptions for Leo I that PK90 used for UMi and Dra, this limit corresponds to  $\sim 0.08 \text{ M}_{\odot} \text{ pc}^{-3}$ . For a stellar  $(M/L)_V$  ratio in the range 0.5-0.8, this limit implies that about 20-50% of the central mass density in Leo I is dark ( $I_{0,V} = 0.097 \text{ L}_{\odot} \text{ pc}^{-3}$ ). Note that in order to achieve such a low *central* mass density for a King-like light profile as observed in Leo I, a considerable amount of mass must be found in an extended halo. Thus, it appears that we cannot use anisotropy in the velocity field to fully eliminate the need for dark matter at all radii. We shall explore this issue in greater detail in Paper III where we analyze individually less precise kinematic results for a larger sample of stars spread over a large radial range in Leo I.

We confirm the large systemic velocity of Leo I reported by Zaritsky et al. (1989) and independently by Kulessa and Lynden-Bell (1992). Interestingly, regardless of the final verdict on the DM content within Leo I, this large radial velocity implies a considerable DM halo about our Galaxy if the dwarf is bound to the Milky Way (Zaritsky et al. 1989;

Kochanek 1996), or a large overall DM content of the Local Group if Leo I is bound to the group as a whole rather than any individual giant galaxy (Byrd et al. 1994). It will be intriguing to determine the relationship, if any, between Leo I’s DM halo and the dark matter that pervades the halo of the Milky Way and the Local Group as a whole.

We close by noting that Leo I is the most distant system for which individual stellar velocities of old red giants have been obtained with a precision of  $\lesssim 2 \text{ km s}^{-1}$ . With the advent of the new generation of 8-10m telescopes, it has become possible to extend these sorts of kinematic studies to the very limit of the Galactic halo, and to start to consider probing further out into the Local Group. Cook et al. (1998) report on a first foray into this realm in their kinematic study of the M 31 satellite LGS 3. It will be exciting to discover if the trends we have begun to see in Galactic satellites hold as we push to more distant systems in different environments and to compare stellar and gas kinematics in low-mass dwarf irregular systems. Perhaps most importantly, it shall be of considerable interest to explore whether there really is a minimum dark-halo mass of approximately  $2 \times 10^7 M_{\odot}$ , and, if so, whether a large population of essentially dark dwarf systems abound in the Local Group and beyond.

## 7. Acknowledgements

MM was partially supported by grants from the NSF during the course of this research. EO was partially supported by NSF grants AST-9223967 and AST-9619524. We would all like to thank the excellent support by the Keck mountain staff, especially Barb Schaeffer, and the UC Keck TAC for providing time to carry out these observations. We thank C. Pryor for sending us his programs to detect rotation and which we used to confirm our independent analysis. We also thanks Denise Hurley-Keller for helping produce Figure 2. Finally, we are grateful to Stacy McGaugh for his careful reading of the manuscript.



## REFERENCES

- Alard, C. 1996, *ApJ*, 458, L17.
- Armandroff, T. E. & Da Costa, G. S. 1986, *AJ*, 92, 777.
- Armandroff, T. E. & Da Costa, G. S. 1991, *AJ*, 101, 1329.
- Armandroff, T. E., Olszewski, E. W., & Pryor, C. 1995, *AJ*, 110, 2131.
- Beers, T. C., Flynn, K., & Gebhardt, K. 1990, *AJ*, 100, 32.
- Bekenstein, J., & Milgrom, M. 1984, *ApJ*, 286, 7.
- Bellazzini, M., Fusi Pecci, F., & Ferraro, F. R. 1996, *MNRAS*, 278, 947.
- Binney, J., & Mamon, G. A. 1982, *MNRAS*, 200, 361.
- Byrd, G., Valtonen, M., McCall, M., & Innanen, K. 1994, *AJ*, 107, 2055.
- Caldwell, N., Armandroff, T. E., Seitzer, P., & Da Costa, G. S. 1992, *AJ*, 103, 840.
- Cook, K. H., Mateo, M., Olszewski, E. W., Stubbs, C. 1998, in preparation.
- Demers, S., Irwin, M. J., & Gambu, I. 1994, *MNRAS*, 266, 7.
- Djorgovski, S., Piotto, G., Phinney, E. S., & Chernoff, D. F. 1991, *ApJ*, 372, L41.
- Elson, R. A. W., Fall, S. M., & Freeman, K. C. 1989, *ApJ*, 336, 734.
- Fahlman, G. G., Mandushev, G., Richer, H. B., Thompson, I. B., & Sivaramakrishnan, A. 1996, *ApJ*, 459, L65.
- Felton, J. E. 1984, *ApJ*, 286, 3.
- Ferraro, F. R., Fusi Pecci, F., Testa, V., Greggio, L., Corsi, C. E., Buonanno, R., Terndrup, D. M., & Zinnecker, H. 1995, *MNRAS*, 272, 391.
- Gallart, C., Freedman, W. L., Mateo, M., Chiosi, C., Thompson, I. et al. 1998, *AJ*, in press.

- Gerhard, O. E. 1994, in *Dwarf Galaxies*, eds. G. Meylan, & P. Prugniel, (Garching: ESO), p. 335.
- Hargreaves, J. C., Gilmore, G., & Annan, J. D. 1996, MNRAS, 279, 108.
- Hargreaves, J. C., Gilmore, G., Irwin, M. J., & Carter, D. 1994, MNRAS, 271, 693.
- Hodge, P. W. 1971, ARAA, 9, 35.
- Ibata, R. A., Wyse, R. F. G., Gilmore, G., Irwin, M. J., & Suntzeff, N. B. 1997, AJ, 113, 634.
- Irwin, M., & Hatzidimitriou, D. 1995, MNRAS, 277, 1354. (IH95)
- Johnston, K. V., Spergel, D. N., & Hernquist, L. 1995, ApJ, 451, 598.
- King, I. R. 1966, AJ, 71, 64.
- Klessen, R. S., & Kroupa, P. 1998, ApJ, 498, 143.
- Kleyna, J. T., Geller, M. J., Kenyon, S. J., Kurtz, M. J., & Thorstensen, J. R. 1998, AJ, 115, 2359.
- Kochanek, C. S. 1996, 457, 228.
- Kormendy, J. 1987, in *Dark Matter in the Universe*, eds. J. Kormendy & G. Knapp, (Dordrecht: Reidel), p. 139.
- Kroupa, P. 1997, NewA, 2, 139.
- Kulessa, A. S. & Lynden-Bell, D. 1992, MNRAS, 255, 105.
- Kuhn, J. R. 1993, ApJ, 409, L13.
- Kuhn, J. R., & Miller, R. H. 1989, ApJ, 341, L41.
- Kuhn, J. R., Smith, H. A., & Hawley, S. L. 1996, ApJ, 469, L93.
- Kuijken, K., & Gilmore, G. 1989, MN, 239, 605.
- Kunkel, W. E. 1979, ApJ, 228, 718.

- Lake, G., & Skillman, E. D. 1989, *AJ*, 98, 1274.
- Lee, M. G., Freedman, W., Mateo, M., Thompson, I., Roth, M., & Ruiz, M. T. 1993, *AJ*, 106, 1420.
- Lo, K. Y., Sargent, W. L. W., & Young, K. 1993, *AJ*, 106, 507.
- Lynden-Bell, D. 1982, *Observatory*, 102, 202.
- Lynden-Bell, D., & Lynden-Bell, R. M. 1995, *MNRAS*, 275, 429.
- Majewski, S. R., 1994, *ApJ*, 431, L17.
- Mateo, M. 1997, in *The Nature of Elliptical Galaxies*, eds. M. Arnaboldi, G. S. Da Costa, & P. Saha, (San Francisco: ASP), p. 259.
- Mateo, M. 1998, *ARAA*, 36, 435.
- Mateo, M., Mirabal, N., Udalski, A., Szymański, M., Kaluzny, J., Kubiak, M., Krzemiński, M., & Stanek, K. Z. 1996, *ApJ*, 458, L13.
- Mateo, M., Olszewski, E. W., Pryor, C., Welch, D. L., & Fischer, P. 1993, *AJ*, 105, 510.
- Mateo, M., Olszewski, E., Welch, D. L., Fischer, P., & Kunkel, W. 1991, *AJ*, 102, 914.
- Mateo, M., Olszewski, E. W., Armandroff, T. E., & Pryor, C. 1998, in preparation. (Paper III)
- McGaugh, S. S., & de Blok, W. J. G. 1998, *ApJ*, 499, 66.
- Mermilliod, J. C. 1981, *A&A*, 97, 235.
- Merritt, D. 1988, *AJ*, 95, 496.
- Milgrom, M. 1983a, *ApJ*, 270, 365.
- Milgrom, M. 1983b, *ApJ*, 270, 371.
- Milgrom, M. 1990, *ApJ*, 367, 490.
- Milgrom, M. 1995, *ApJ*, 455, 439.

- Milgrom, M. 1998, ApJ, 496, L89.
- Oh, K. S., Lin, D. N. C., & Aarseth, S. J. 1995, ApJ, 442, 142.
- Olszewski, E. W. 1998, in *Santa Cruz Workshop on Galaxy Halos*, ed. D. Zaritsky, (San Francisco: ASP), p. 70.
- Olszewski, E. W., Aaronson, M., & Hill, J. M. 1995, AJ, 110, 2120.
- Olszewski, E. W., Pryor, C., & Armandroff, T. E. 1996, AJ, 111, 750.
- Paltoglou, G., & Freeman, K. C. 1987, in *Structure and Dynamics of Elliptical Galaxies*, ed. T. de Zeeuw, (Dordrecht: Reidel), p. 447.
- Peebles, P. J. E. 1989, ApJ, 344, L53.
- Peebles, P. J. E. 1995, ApJ, 449, 52.
- Piatek, S., & Pryor, C. 1995, AJ, 109, 1071.
- Pryor, C. 1992, in *Morphological and Physical Classification of Galaxies*, eds. G. Longo, M. Capaccioli, & G. Busarello, (Dordrecht: Kluwer), p. 163.
- Pryor, C. 1996, in *Formation of the Galactic Halo . . . Inside and Out*, eds. H. Morrison, & A. Sarajedini, (San Francisco: ASP), Vol 92, p 424.
- Pryor, C., & Kormendy J. 1990, AJ, 100, 127. (PK90)
- Pryor, C., & Meylan, G. 1993, in *Structure and Dynamics of Globular Clusters*, eds. S. G. Djorgovski, & G. Meylan, (San Francisco: ASP), p. 357.
- Queloz, D., Dubath, P., & Pasquini, L. 1995, A&A, 300, 31.
- Richstone, D. O., & Tremaine, S. 1986, AJ, 92, 72.
- Sanders, R. H. 1997, ApJ, 480, 492.
- Shara, M. M., Drissen, L., Rich, R. M., Paresce, F., King, I. R., & Meylan, G. 1998, ApJ, 495, 796.

Tonry, J., & Davis, M. 1979, AJ, 84, 1511.

Vogt, S., Allen, S., Bigelow, B., Bresee, L., Brown, B., Cantrall, T., Conrad, A., et al. 1994, Proc SPIE, 2198, 362.

Vogt, S.S., Mateo, M., Olszewski, E.W., & Keane, M. J. 1995, AJ, 109, 151. (Paper I)

Young, L. M., & Lo, K. Y. 1996a, ApJ, 462, 203.

Young, L. M., & Lo, K. Y. 1997a, ApJ, 476, 127.

Young, L. M., & Lo, K. Y. 1997b, ApJ, 490, 710.

Zaritsky, D., Olszewski, E. W., Schommer, R. A., Peterson, R. C., Aaronson, M. 1989, ApJ, 345, 759.

### Figure Captions

**Figure 1** – A color-magnitude diagram of bright stars in the central region of Leo I. The region from which we extracted candidate Leo I red giant members is enclosed by the dashed line; the 33 stars that we observed spectroscopically are shown as large solid squares.

**Figure 2** – A finding chart of the stars observed spectroscopically in Leo I. The numbers refer to the star IDs listed in Table 2. The field is approximately  $4.9 \times 5.1$  arcmin along the horizontal and vertical axes, respectively. North is towards the bottom, and east is towards the left. Star 15 is the northern most star in the compact grouping in which it is located, while star 17 is the southern star of a close pair. The center of the field is located at  $\alpha_{2000} = 10^h08^m27.93^s$ ,  $\delta_{2000} = 12^\circ18'18.4''$ .

**Figure 3** – The distribution of velocities of the 33 stars observed spectroscopically. There are no obvious outliers in the sample.

**Figure 4** – Plots of the observed heliocentric radial velocities of the 33 Leo I stars in our sample vs radial distance from the galaxy center (*upper left*), position angle relative to the galaxy center (*upper right*), the (V–I) colors of the stars (*lower left*), and the apparent I-band magnitude of the stars (*lower right*). There are no significant correlations of the mean velocity or velocity dispersion with respect to any of these variables.

**Figure 5** – *Top panel* A plot of the observed heliocentric radial velocities vs the radial distance projected along the axis with the strongest rotational signal as determined using the least-squares procedure described in Section 3.2 (see the discussion related to equation 2). The slope of the velocity gradient is shown along with the 2-sigma error bars. The range

enclosed by the error bars includes a slope of zero, meaning that the data do not reveal any significant evidence of rotation in the central region of Leo I. *Lower panel* The variation of the reduced  $\chi^2$  as a function of position angle about the center of Leo I for equation 2. This angle measures the direction of the maximum velocity gradient due to rotation. Although there is a broad minimum centered at  $\text{PA} \sim 54^\circ$ , the large value of  $\chi^2$  and the small range of variation of this statistic over the full range of PA values is another indication that we have not detected a significant rotation signal in Leo I. For comparison, the major axis position angle is  $79^\circ \pm 3^\circ$  (Table 4).

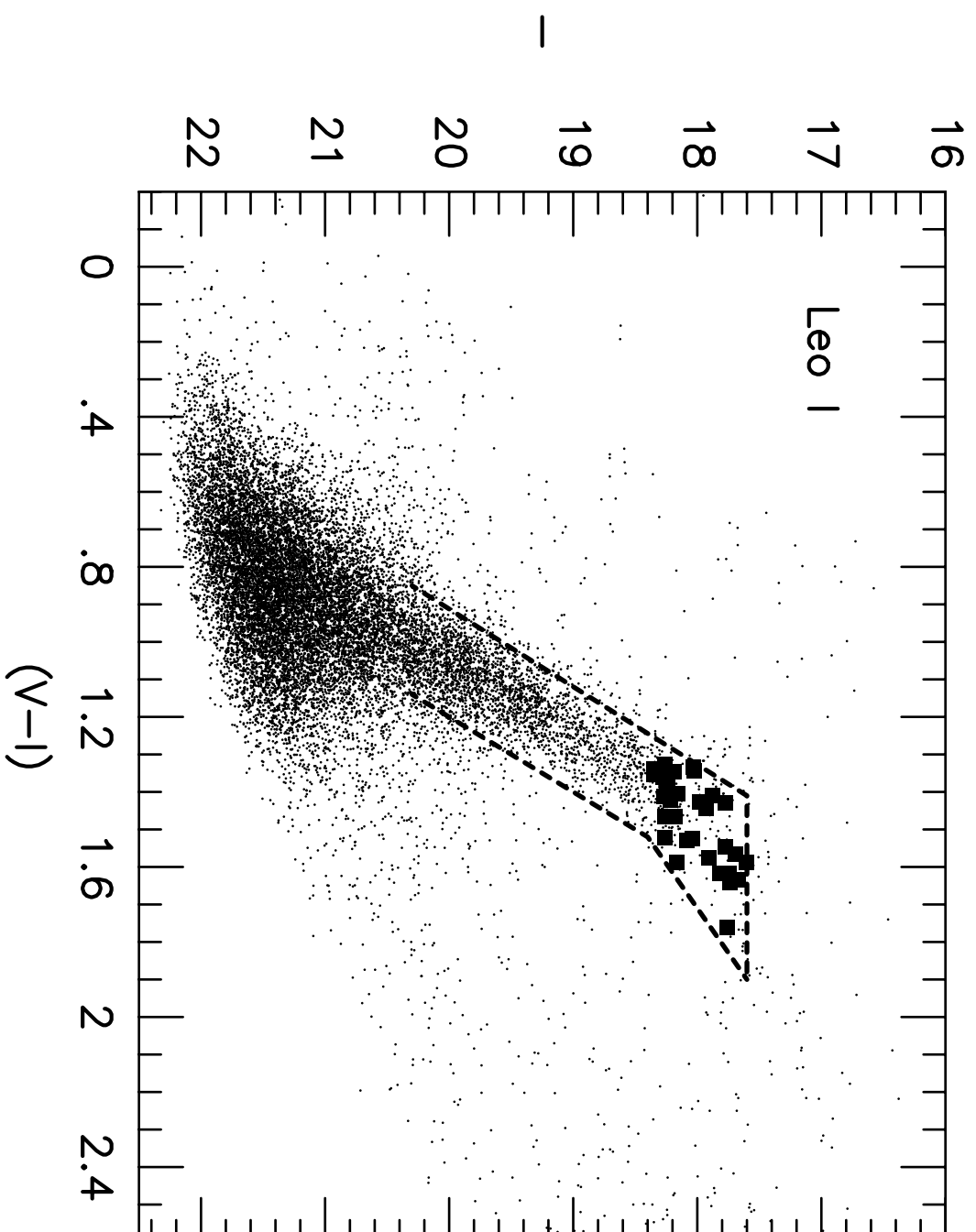
**Figure 6** – Plots of the adopted star-formation histories (SFH) of a selected set of objects. The upper row shows the SFHs of Leo I, a hypothetical globular cluster, and a ‘young’ population (see details in Section 5.1 for details). Rows 2-3 show the SFHs of the other eight Galactic dSph satellites. In all cases, only relative star-formation rates are plotted and time is shown in units of Gyr where we have assumed the oldest possible population has an age of 14 Gyr. These SFHs are used to calculate the  $(M/L)$  correction factors described in section 5.1 and listed in Tables 6 and 7. The SFHs adopted here for the galaxies are taken from Mateo (1998).

**Figure 7** – *Top panel* The variation of the ‘total’ V-band mass-to-light ratio of Galactic and M 31 dSph systems as a function of visual absolute magnitude. The data for the other galaxies are taken from Mateo (1998) and Kleyna et al. (1998). *Lower panel* The same plot but now where the  $(M/L)$  ratios and absolute magnitudes have been corrected for stellar evolutionary effects as described in section 5.1 and using the star-formation histories plotted in Figure 6. We have applied no corrections in this panel for the three M 31 satellites: NGC 147, NGC 185, and NGC 205. In both plots the dashed lines correspond to equation 7 with  $(M/L)_s = 1.5$ , and  $M_0 = 2.0 \times 10^7 M_\odot$ . We have adopted the results of Ibata et al.

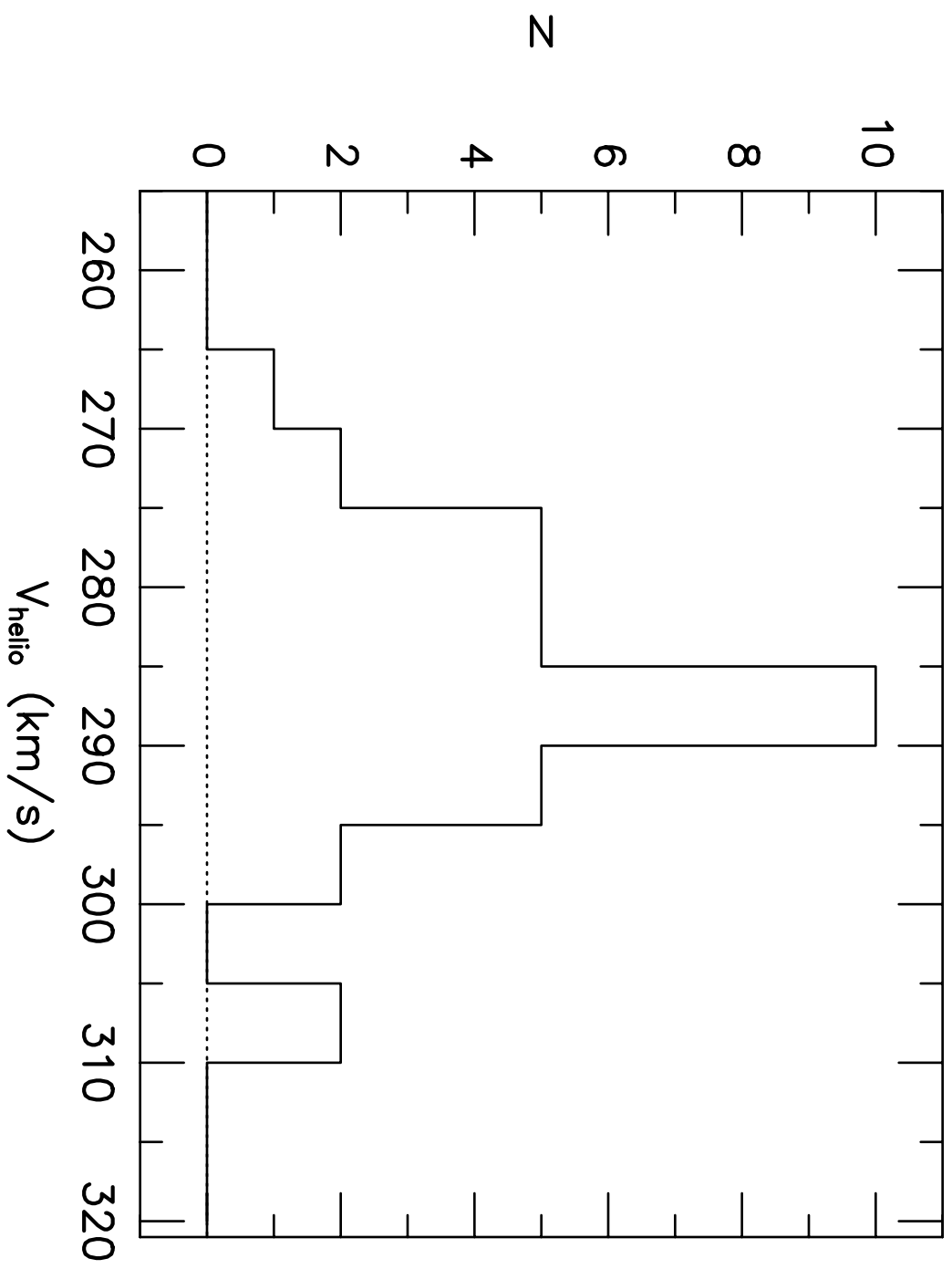
(1997) for Sgr; their analysis assumes that Sgr is in dynamical equilibrium despite some evidence to the contrary (Bellazzini et al. 1996; Mateo 1998). The points for Sgr should be regarded as upper limits to the true ( $M/L$ ) ratio of that galaxy.



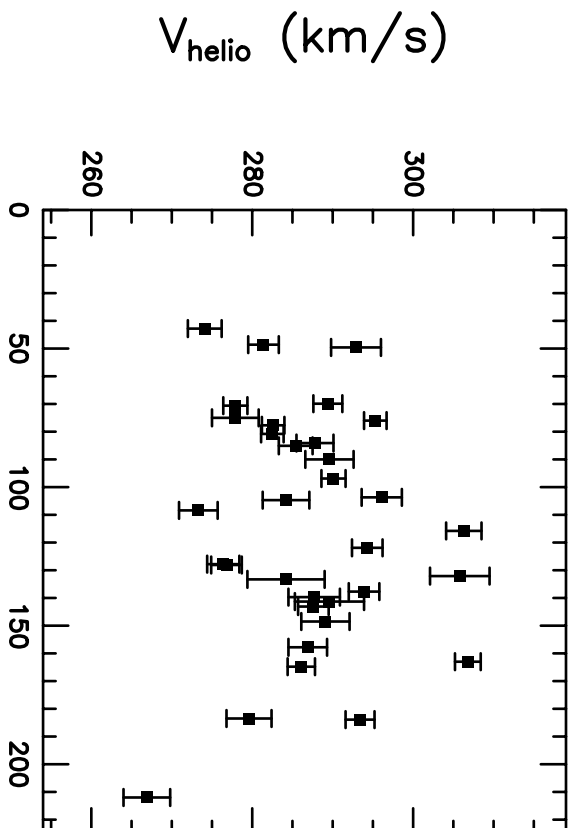
Mateo et al – Figure 1



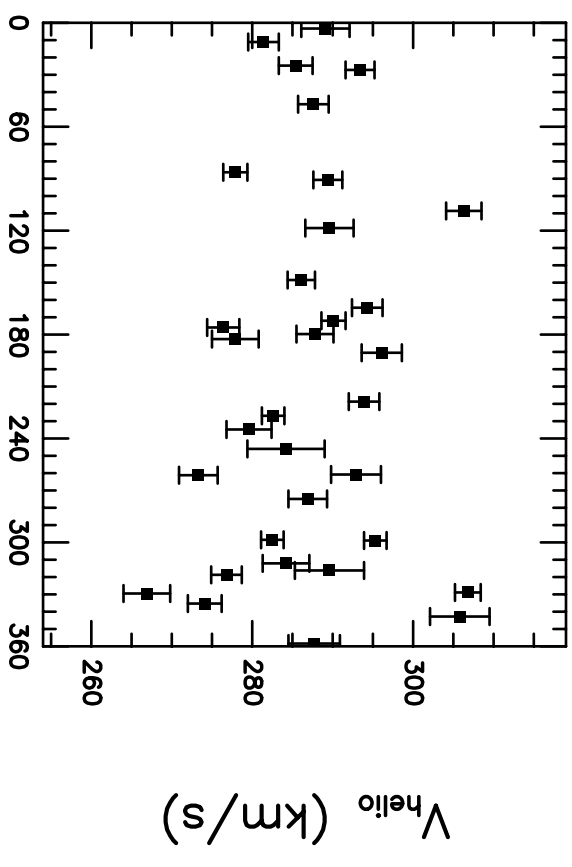
Mateo et al – Figure 3



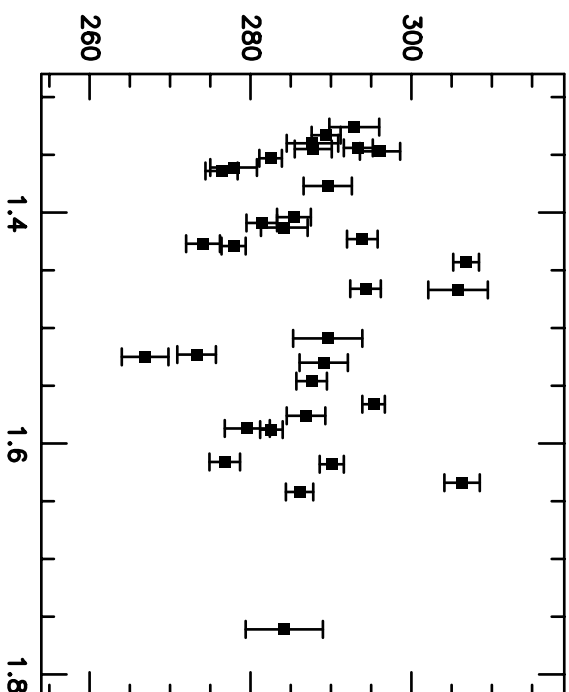
R (arcsec)



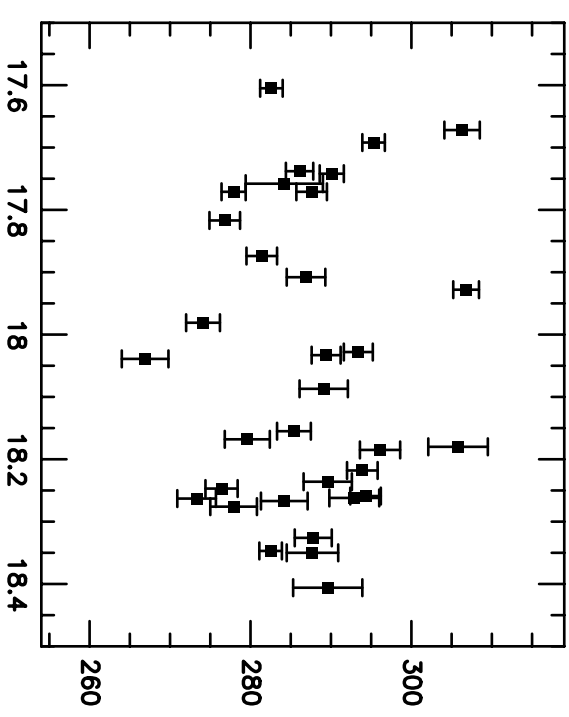
PA (degrees)



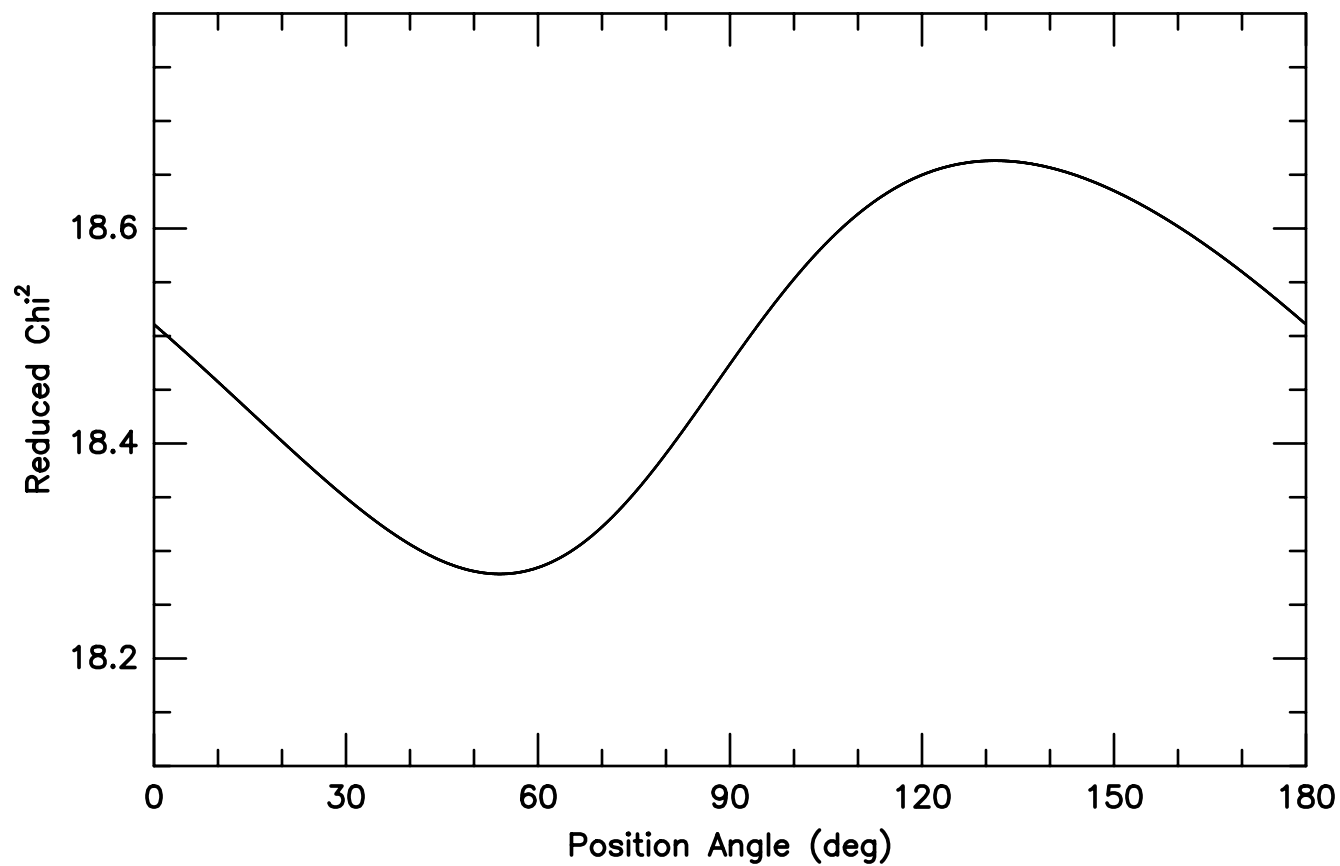
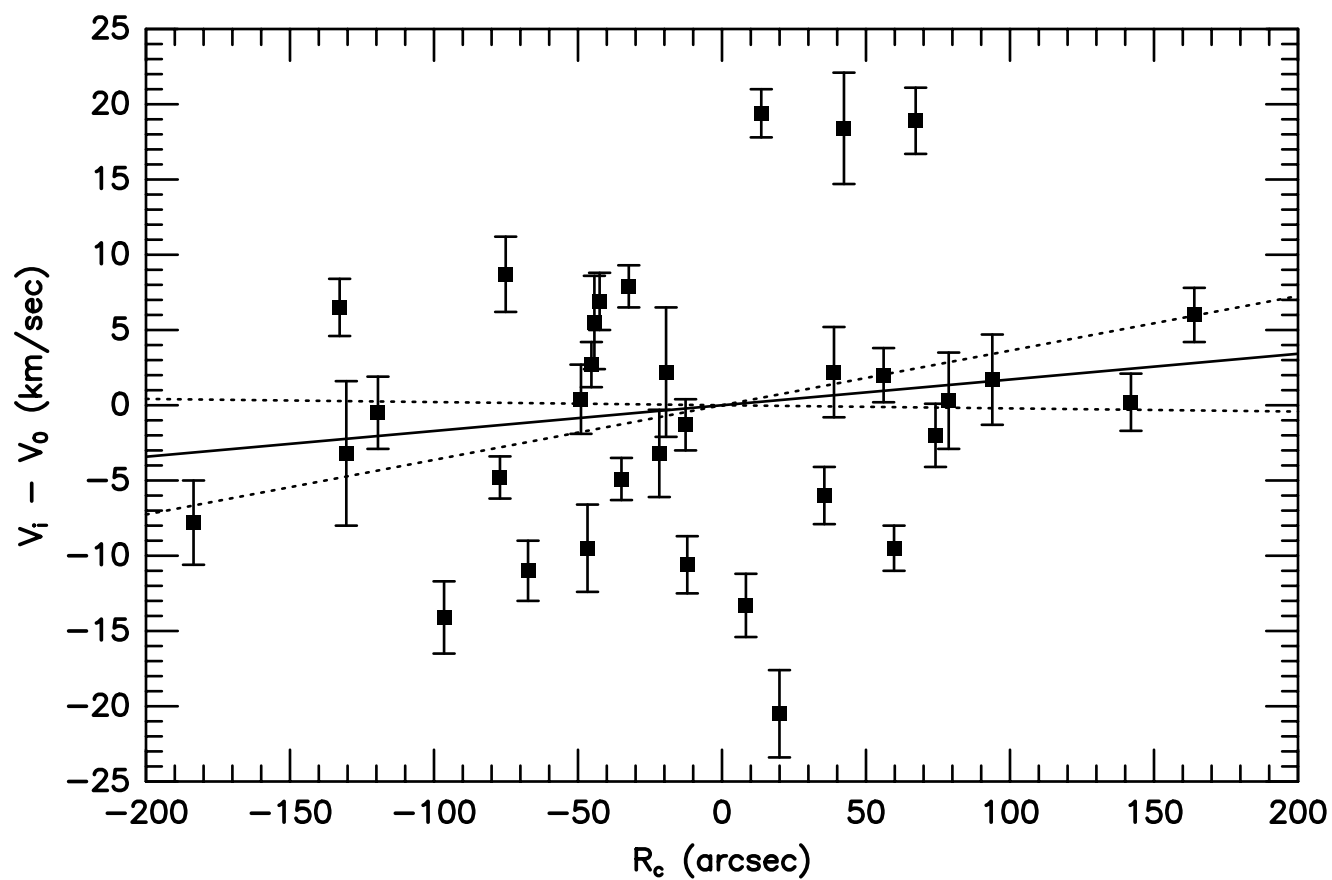
$V_{\text{helio}}$  (km/s)



$V_{\text{helio}}$  (km/s)

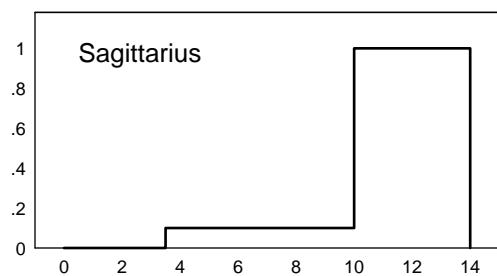
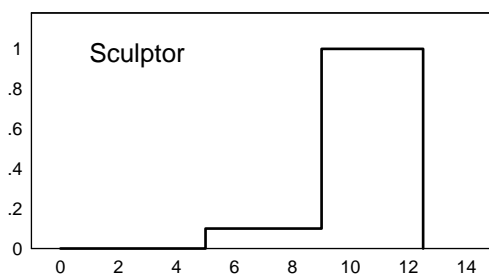
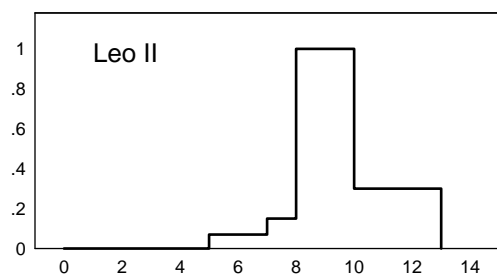
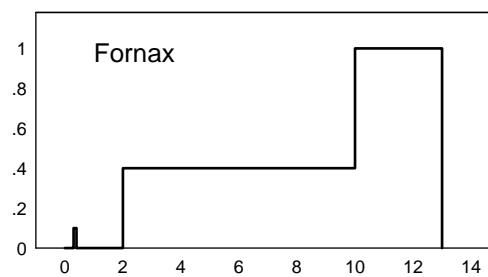
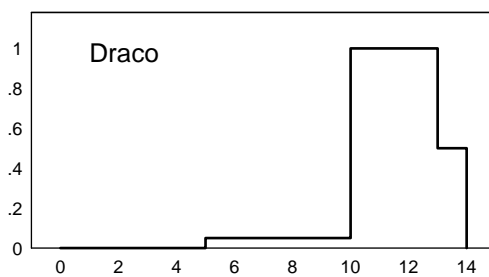
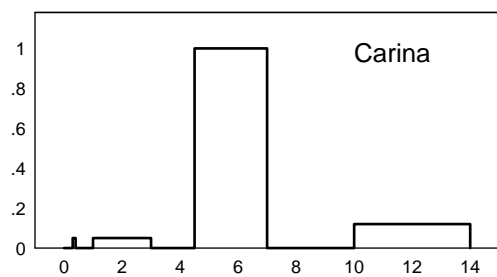
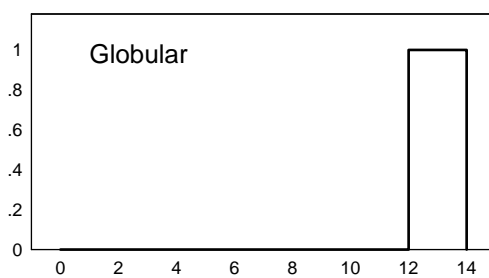
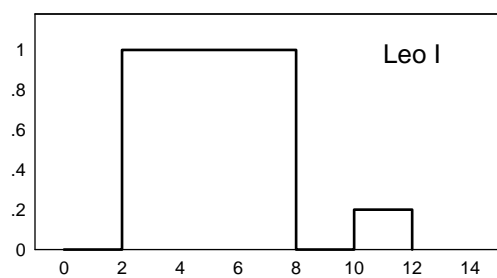


Mateo et al – Figure 5



Mateo et al - Figure 6

Relative SFR



Age (Gyr)

Mateo et al – Figure 7

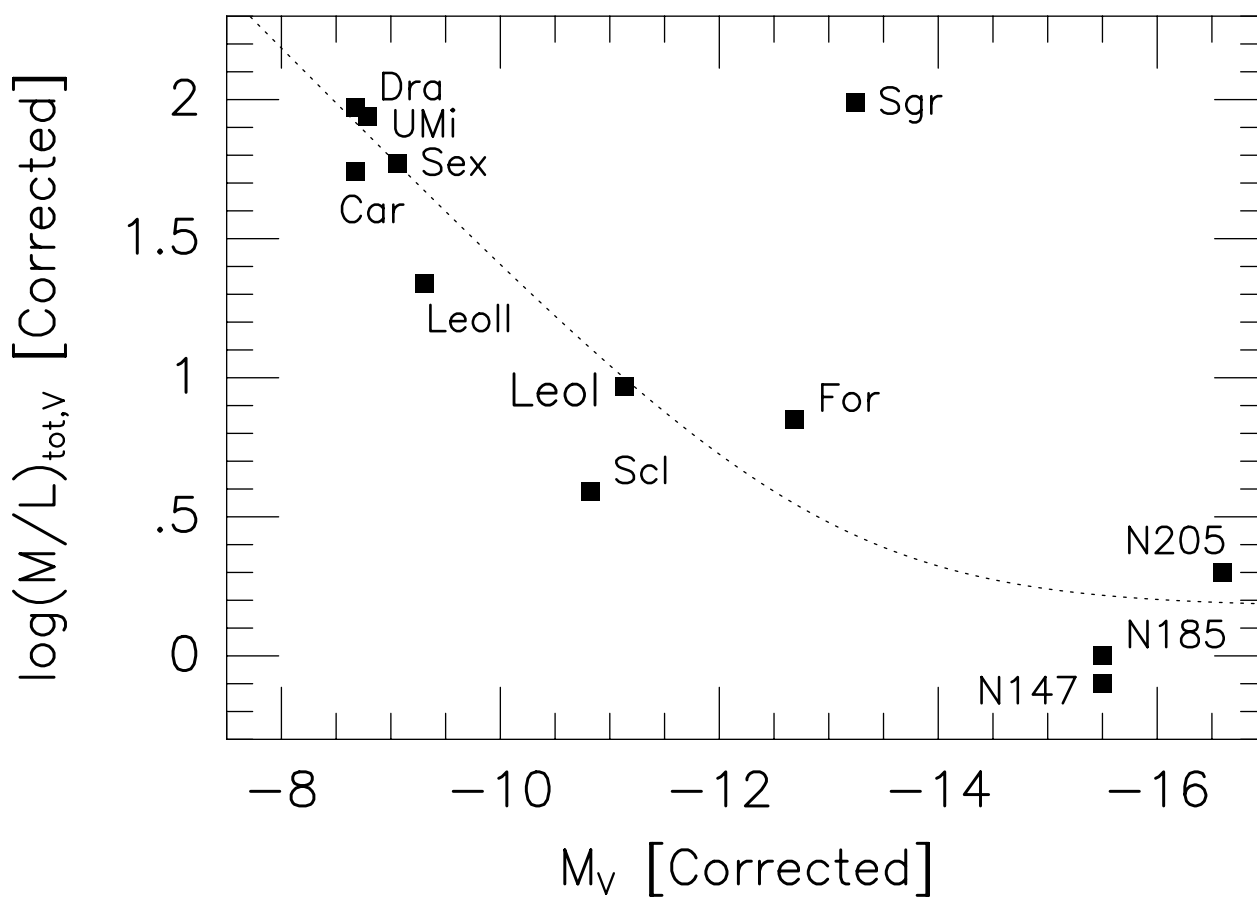
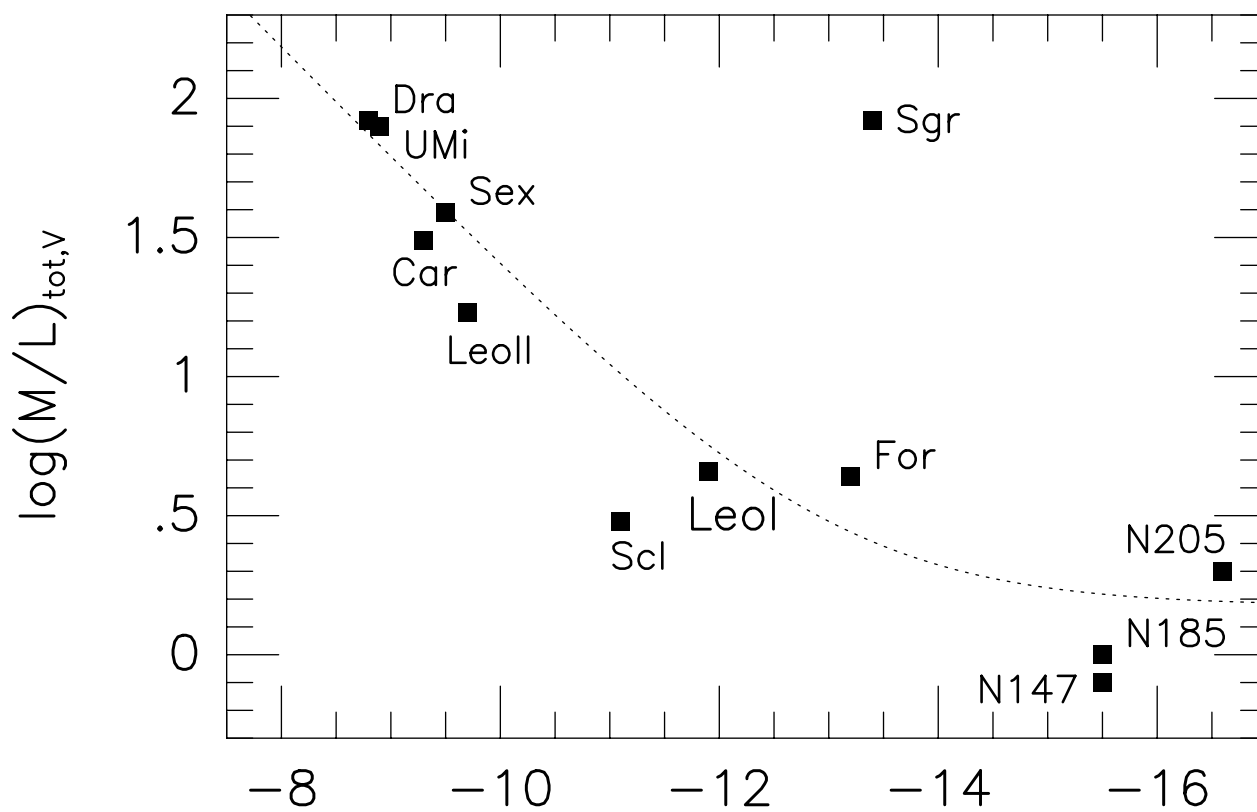


Table 1. Log of Leo I Kinematic Observations

Star	UT Date	UT <sub>mid</sub>	ET sec	Airmass	HJD <sub>mid</sub> –2450000.0	$V_h$ km s <sup>–1</sup>	$R$
23	13 Mar 1996	08 13 08	600	1.04	155.84800	283.3	9.3
15	13 Mar 1996	08 31 39	660	1.02	155.86100	295.1	10.0
14	13 Mar 1996	08 49 01	900	1.01	155.87306	281.6	10.0
5	13 Mar 1996	11 22 55	750	1.19	155.97998	306.8	7.5
20	13 Mar 1996	11 51 55	900	1.29	155.99999	273.2	5.2
15	14 Mar 1996	05 34 32	300	1.58	156.73799	296.1	5.0
19	14 Mar 1996	05 44 00	450	1.52	156.74449	292.9	3.3
24	14 Mar 1996	05 52 54	300	1.45	156.75059	284.2	1.8
21	14 Mar 1996	06 02 29	300	1.39	156.75728	306.3	5.2
28	14 Mar 1996	06 14 50	450	1.36	156.76575	296.1	4.4
22	14 Mar 1996	06 26 43	450	1.30	156.77409	289.6	3.4
16	14 Mar 1996	06 38 11	450	1.25	156.78215	286.9	4.5
12	14 Mar 1996	06 50 48	450	1.21	156.79097	281.4	6.2
27	14 Mar 1996	07 00 56	450	1.17	156.79777	290.1	7.7
17	14 Mar 1996	07 13 40	450	1.14	156.80678	277.9	7.9
33	14 Mar 1996	07 24 11	450	1.12	156.81385	286.1	7.0
23	14 Mar 1996	07 42 34	450	1.08	156.82675	281.6	7.9
13	14 Mar 1996	07 54 34	450	1.06	156.83524	274.1	5.4
21	14 Mar 1996	08 08 16	450	1.04	156.84463	306.4	5.9
22	14 Mar 1996	08 18 18	450	1.03	156.85158	290.6	3.6
10	14 Mar 1996	08 32 10	450	1.02	156.86139	285.4	5.4
18	14 Mar 1996	08 41 52	450	1.02	156.86802	289.4	6.5
1	14 Mar 1996	08 56 31	450	1.01	156.87832	266.9	3.7
2	14 Mar 1996	09 07 10	450	1.01	156.88571	293.4	6.3
30	14 Mar 1996	09 18 39	450	1.01	156.89338	293.9	6.2
11	14 Mar 1996	09 29 05	450	1.01	156.90091	284.2	3.6
29	14 Mar 1996	09 39 22	450	1.02	156.90777	279.6	3.8
8	14 Mar 1996	09 50 44	450	1.02	156.91596	287.6	6.0

Table 1—Continued

Star	UT Date	UT <sub>mid</sub>	ET sec	Airmass	HJD <sub>mid</sub> −2450000.0	$V_h$ km s <sup>−1</sup>	$R$
20	14 Mar 1996	10 01 51	450	1.03	156.92353	273.6	3.5
14	14 Mar 1996	10 15 00	450	1.05	156.93276	286.4	4.4
14	14 Mar 1996	10 35 26	600	1.08	156.94695	286.0	5.3
25	14 Mar 1996	10 48 51	600	1.11	156.95607	277.9	3.6
26	14 Mar 1996	11 01 06	600	1.14	156.96457	287.8	4.9
32	14 Mar 1996	11 16 29	600	1.18	156.97518	276.4	5.8
31	14 Mar 1996	11 28 47	600	1.22	156.98374	294.3	6.2
3	14 Mar 1996	11 41 20	600	1.27	156.99277	289.1	3.5
4	14 Mar 1996	11 54 19	600	1.33	157.00179	287.7	3.2
6	14 Mar 1996	12 10 29	600	1.41	157.01302	305.8	2.6
9	14 Mar 1996	12 23 10	600	1.49	157.02181	276.8	6.2
7	14 Mar 1996	12 35 12	600	1.58	157.03017	289.6	2.1



Table 2. Positions and Kinematics of Observed Leo I Stars

Star	$\alpha_{2000}$	$\delta_{2000}$	I mag	(V–I) mag	$\langle v_h \rangle$ km s <sup>–1</sup>	$\delta_v$ km s <sup>–1</sup>	$N$	$r$ arcsec	PA deg
1	10 08 20.6	+12 21 03	18.04	1.53	266.9	2.9	1	212.0	329.5
2	10 08 33.7	+12 20 44	18.03	1.34	293.4	1.8	1	183.9	27.2
3	10 08 28.5	+12 20 28	18.09	1.53	289.1	3.0	1	148.5	3.3
4	10 08 27.7	+12 20 20	18.35	1.34	287.7	3.2	1	139.7	358.4
5	10 08 22.2	+12 20 20	17.93	1.44	306.8	1.6	1	163.0	328.9
6	10 08 25.3	+12 20 06	18.18	1.47	305.8	3.7	1	132.1	342.8
7	10 08 21.3	+12 19 42	18.41	1.51	289.6	4.3	1	141.3	316.2
8	10 08 35.1	+12 19 38	17.77	1.55	287.6	1.9	1	143.1	47.0
9	10 08 22.2	+12 19 36	17.82	1.62	276.8	1.9	1	128.1	318.7
10	10 08 30.4	+12 19 17	18.16	1.40	285.4	2.1	1	85.1	24.7
11	10 08 22.6	+12 19 10	18.27	1.41	284.2	2.9	1	104.7	312.1
12	10 08 28.6	+12 18 48	17.87	1.41	281.4	1.9	1	48.6	11.1
13	10 08 26.7	+12 18 39	17.98	1.43	274.1	2.1	1	42.8	335.3
14	10 08 23.1	+12 18 39	18.35	1.35	282.5	1.4	3	80.8	298.5
15	10 08 23.4	+12 18 37	17.69	1.57	295.3	1.4	2	76.0	298.9
16	10 08 17.2	+12 18 13	17.91	1.58	286.9	2.4	1	157.8	274.9
17	10 08 32.7	+12 18 05	17.77	1.43	277.9	1.5	1	70.6	86.3
18	10 08 32.7	+12 17 59	18.03	1.33	289.4	1.8	1	69.9	90.7
19	10 08 24.6	+12 17 52	18.26	1.33	292.9	3.1	1	49.6	260.8
20	10 08 20.6	+12 17 43	18.26	1.52	273.3	2.4	2	108.4	261.2
21	10 08 35.4	+12 17 23	17.67	1.63	306.3	2.2	2	115.8	108.6
22	10 08 33.3	+12 17 17	18.24	1.38	289.6	3.0	2	90.0	118.5
23	10 08 24.1	+12 17 07	17.61	1.59	282.6	1.4	2	77.7	226.9
24	10 08 19.6	+12 17 06	17.76	1.76	284.2	4.8	1	133.3	246.0
25	10 08 27.7	+12 16 45	18.28	1.36	277.9	2.9	1	75.0	182.6
26	10 08 28.0	+12 16 36	18.33	1.35	287.8	2.3	1	84.1	179.7
27	10 08 28.9	+12 16 24	17.74	1.62	290.1	1.5	1	96.9	172.0
28	10 08 26.6	+12 16 18	18.19	1.35	296.1	2.5	1	103.7	190.5
29	10 08 17.7	+12 16 14	18.17	1.59	279.6	2.8	1	183.5	234.8
30	10 08 22.1	+12 16 12	18.22	1.42	293.9	1.9	1	137.7	218.7
31	10 08 30.2	+12 16 03	18.26	1.47	294.3	1.9	1	121.9	164.5
32	10 08 28.6	+12 15 53	18.25	1.36	276.4	2.0	1	127.8	175.9
33	10 08 33.8	+12 15 39	17.74	1.64	286.1	1.7	1	164.8	148.5

Table 3. Velocity Dispersions and Systemic Velocities of Leo I Subsamples

Subsample	$N$	Weighted Mean		Bi-weight		Max Likelihood	
		$\sigma_v$ km s <sup>-1</sup>	$\langle v \rangle$ km s <sup>-1</sup>	$\sigma_v$ km s <sup>-1</sup>	$\langle v \rangle$ km s <sup>-1</sup>	$\sigma_v$ km s <sup>-1</sup>	$\langle v \rangle$ km s <sup>-1</sup>
All Stars	33	$8.6 \pm 1.2$	$287.3 \pm 1.6$	$9.2 \pm 1.6$	$286.7 \pm 2.0$	$8.8 \pm 1.3$	$287.0 \pm 1.6$
AGB Stars	18	$9.3 \pm 1.8$	$287.8 \pm 2.3$	$9.6 \pm 2.3$	$286.4 \pm 2.8$	$9.6 \pm 1.9$	$287.0 \pm 2.3$
RGB Stars	15	$7.2 \pm 1.7$	$286.2 \pm 2.0$	$8.4 \pm 2.2$	$286.9 \pm 2.9$	$7.8 \pm 1.6$	$287.0 \pm 2.2$
Inner Third	11	$6.0 \pm 1.6$	$284.4 \pm 2.0$	$6.5 \pm 2.0$	$284.2 \pm 2.9$	$5.9 \pm 1.5$	$284.3 \pm 2.3$
Middle Third	11	$10.0 \pm 2.6$	$288.0 \pm 3.2$	$11.3 \pm 3.4$	$288.5 \pm 3.8$	$10.4 \pm 2.7$	$288.8 \pm 3.0$
Outer Third	11	$9.2 \pm 2.4$	$290.8 \pm 3.0$	$4.7 \pm 1.4$	$288.6 \pm 2.5$	$9.0 \pm 2.3$	$288.1 \pm 2.8$
Inner Half	16	$6.3 \pm 1.4$	$285.1 \pm 1.7$	$7.2 \pm 1.8$	$285.0 \pm 2.5$	$6.4 \pm 1.4$	$285.0 \pm 2.0$
Outer Half	17	$10.3 \pm 2.0$	$290.0 \pm 2.6$	$10.9 \pm 2.6$	$288.6 \pm 3.0$	$10.3 \pm 2.1$	$288.9 \pm 2.4$
East Half	16	$10.1 \pm 2.1$	$288.8 \pm 2.7$	$11.2 \pm 2.8$	$288.5 \pm 3.2$	$10.5 \pm 2.2$	$288.8 \pm 2.5$
West Half	17	$6.6 \pm 1.4$	$285.8 \pm 1.7$	$7.2 \pm 1.7$	$285.3 \pm 2.5$	$6.6 \pm 1.4$	$285.3 \pm 1.9$
Random 5%	11	5.2	283.2	5.3	282.9	5.3	283.3
Random 95%	11	11.0	291.4	12.0	290.4	11.2	290.8
Random 5%	16	6.1	284.3	6.4	284.0	6.3	284.3
Random 95%	16	10.4	290.2	11.2	289.4	10.6	289.8

Table 4. Structural and Kinematic Parameters for Leo I

Quantity	Symbol	Value	Units	Source <sup>1</sup>
Observed Structural and Kinematic Parameters				
Distance	$D$	$251 \pm 25$	kpc	L93, D94
Distance Modulus	$(m - M)_0$	$22.0 \pm 0.2$	mag	
Core Radius <sup>2</sup>	$r_c$	$3.3 \pm 0.3$	arcmin	IH95
Tidal Radius <sup>2</sup>	$r_t$	$12.6 \pm 1.5$	arcmin	IH95
Half-Light Radius <sup>2</sup>	$r_{1/2}$	$2.6 \pm 0.3$	arcmin	IH95
Ellipticity	$e$	$0.21 \pm 0.03$		IH95
Major Axis PA	PA	$79 \pm 3$	degrees	IH95
Central Surface Brightness, V	$\Sigma_{0,V}$	$22.4 \pm 0.3$	mag arcsec <sup>-2</sup>	C92, IH95
Central Surface Brightness, B	$\Sigma_{0,B}$	$23.2 \pm 0.4$	mag arcsec <sup>-2</sup>	C92, IH95
Central Velocity Dispersion	$\sigma_0$	$8.8 \pm 1.3$	km sec <sup>-1</sup>	Table 3
Derived Structural Parameters				
Absolute Magnitude, V	$M_V$	$-11.9 \pm 0.3$	mag	IH95
Absolute Magnitude, B	$M_B$	$-11.1 \pm 0.4$	mag	IH95
True Core Radius <sup>2</sup>	$R_c$	$240 \pm 25$	pc	
True Tidal Radius <sup>2</sup>	$R_t$	$920 \pm 110$	pc	
True Half-Light Radius <sup>2</sup>	$R_{1/2}$	$190 \pm 22$	pc	
Concentration	$c \equiv \log_{10}(R_t/R_c)$	$0.58 \pm 0.07$		
Surface Brightness, V	$S_{0,V}$	$39 \pm 11$	$L_{\odot V} \text{ pc}^{-2}$	
Surface Brightness, B	$S_{0,B}$	$32 \pm 14$	$L_{\odot B} \text{ pc}^{-2}$	
Model-Dependent Parameters				
Scale Factor, Eqn 3	$\eta$	0.96		RT86
Scale Factor, Eqn 5	$\beta$	3.9		K66
Velocity Scale Factor	$v_s/\sigma_0$	1.48		K66, PK90
Scale Velocity	$v_s$	$13.0 \pm 1.9$	km sec <sup>-1</sup>	Table 3

<sup>1</sup>IH95 = Irwin and Hatzidimitriou 1995; L93 = Lee et al. 1993; D94 = Demers et al. 1994; C92 = Caldwell et al. 1992; RT = Richstone and Tremaine 1986; K66 = King 1966; PK = Pryor and Kormendy 1990.

<sup>2</sup>Geometric mean radius:  $r_{geom} = r_{maj}(1 - e)^{1/2}$ , and  $e$  is the ellipticity.

Table 5. Derived Dynamical Properties of Leo I

Quantity	Symbol	Value	Units	Source
Central Mass Density	$\rho_0$	$0.34 \pm 0.09$	$\text{M}_\odot \text{pc}^{-3}$	Eqn 3
Total Mass	$M_{tot}$	$2.7 \pm 0.6 \times 10^7$	$\text{M}_\odot$	Eqn 4
Central Luminosity Density, V	$I_{0,V}$	$0.097 \pm 0.030$	$\text{L}_{\odot V} \text{pc}^{-3}$	Eqn 5
Central $(M/L)$ Ratio, V	$\rho_0/I_{0,V} \equiv (M/L)_{0,V}$	$3.5 \pm 1.4$	$\text{M}_\odot/\text{L}_{\odot V}$	
‘Total’ Luminosity, V	$L_{tot,V}$	$4.8 \pm 1.5 \times 10^6$	$\text{L}_{\odot V}$	Table 4
‘Total’ $(M/L)$ Ratio, V	$(M_{tot}/L_{tot,V})_V$	$5.6 \pm 2.1$	$\text{M}_\odot/\text{L}_{\odot V}$	
Central Luminosity Density, B	$I_{0,B}$	$0.046 \pm 0.021$	$\text{L}_{\odot B} \text{pc}^{-3}$	Eqn 5
Central $(M/L)$ Ratio, B	$\rho_0/I_{0,B} \equiv (M/L)_{0,B}$	$7.4 \pm 3.9$	$\text{M}_\odot/\text{L}_{\odot B}$	
‘Total’ Luminosity, B	$L_{tot,B}$	$4.0 \pm 1.8 \times 10^6$	$\text{L}_{\odot B}$	Table 4
‘Total’ $(M/L)$ Ratio, B	$(M_{tot}/L_{tot,B})_B$	$6.8 \pm 3.4$	$\text{M}_\odot/\text{L}_{\odot B}$	

Table 6. Stellar Mass-to-Light Ratios and Adjustment Factors for Galactic dSph Systems

Galaxy	Mass Function	$(M/L)_s$	$\lambda$
Globular	Salpeter	1.36	1.00
	Composite	1.56	1.00
Young	Salpeter	0.22	6.18
	Composite	0.37	4.22
Leo I	Salpeter	0.59	2.31
	Composite	0.89	1.75
Carina	Salpeter	0.68	2.00
	Composite	1.01	1.54
Draco	Salpeter	1.15	1.18
	Composite	1.48	1.05
Fornax	Salpeter	0.77	1.77
	Composite	1.10	1.42
Leo II	Salpeter	0.95	1.43
	Composite	1.38	1.13
Sculptor	Salpeter	1.02	1.33
	Composite	1.44	1.08
Sextans	Salpeter	0.98	1.39
	Composite	1.32	1.18
Sagittarius	Salpeter	1.11	1.16
	Composite	1.43	1.09
Ursa Minor	Salpeter	1.16	1.17
	Composite	1.48	1.05